Geophysical Research Letters

RESEARCH LETTER
10.1029/2022GL099366

Key Points:

- Single-crystal elasticity of α- and β-orthopyroxene was determined to 20 GPa and shows anomalous change across the phase transition
- The obtained results were used to model the velocity profiles of the coldest harzburgite layer of the sinking subduction slab
- We find that the low-velocity anomalies within the slab at the top transition zone should be caused by metastable orthopyroxene and olivine

Supporting Information:

Supporting Information may be found in the online version of this article.

Correspondence to:

Z. Mao,
zhumao@ustc.edu.cn

Citation:

Li, L., Sun, N., Shi, W., Mao, Z., Yu, Y., Zhang, Y., & Lin, J.-F. (2022). Elastic anomalies across the α-β phase transition in orthopyroxene: Implication for the metastable wedge in the cold subduction slab. *Geophysical Research Letters*, *49*, e2022GL099366. https://doi.org/10.1029/2022GL099366

Received 30 APR 2022
Accepted 28 JUL 2022

Author Contributions:

Conceptualization: Zhu Mao
Data curation: Luo Li, Weigang Shi, Yingxin Yu
Formal analysis: Luo Li, Ningyu Sun, Weigang Shi
Funding acquisition: Zhu Mao
Investigation: Luo Li
Methodology: Luo Li, Ningyu Sun, Weigang Shi, Yingxin Yu
Project Administration: Zhu Mao
Resources: Luo Li
Software: Luo Li, Ningyu Sun, Weigang Shi, Yingxin Yu
Validation: Luo Li
Visualization: Luo Li, Ningyu Sun
Writing – original draft: Luo Li, Zhu Mao

Elastic Anomalies Across the α-β Phase Transition in Orthopyroxene: Implication for the Metastable Wedge in the Cold Subduction Slab

Luo Li[1], Ningyu Sun[1,2,3], Weigang Shi[1], Zhu Mao[1,2,3], Yingxin Yu[1], Yanyao Zhang[4], and Jung-Fu Lin[4]

[1]Laboratory of Seismology and Physics of Earth's Interior, School of Earth and Space Sciences, University of Science and Technology of China, Hefei, China, [2]CAS Center for Excellence in Comparative Planetology, University of Science and Technology of China, Hefei, China, [3]Frontiers Science Center for Planetary Exploration and Emerging Technologies, University of Science and Technology of China, Hefei, China, [4]Department of Geological Sciences, Jackson School of Geosciences, The University of Texas at Austin, Austin, TX, USA

Abstract Single-crystal elasticity of both α- and β-orthopyroxene was determined up to 20 GPa and 300 K by Brillouin scattering. Using the derived full elastic moduli (C_{ij}), we investigated the contribution of the metastable pyroxene to the seismically observed 3%–5% low-velocity anomalies along the subducting slab in the top transition zone. Our modeled results show that a harzburgite wedge with a 1000-K colder geotherm and metastable α-orthopyroxene and olivine displays compressional (V_P) and shear-wave (V_S) velocities 3.0%–3.6(6)% and 2.0%–2.8(6)% lower than the surrounding mantle at 410–460 km depth, respectively. At deeper depth up to 520 km, V_P and V_S of this metastable wedge with β-orthopyroxene and olivine are 3.6%–4.4(6)% and 2.8%–4.3(6)% lower than the pyrolitic mantle, respectively. The presence of both metastable orthopyroxene and olivine instead of metastable olivine alone helps better explain the origin of the low-velocity anomalies within the subduction slab in the top transition zone.

Plain Language Summary Subducting slab plays a significant role in transportation the surface material to the Earth's deep interior. It is normally imaged as a high-velocity body compared to the surrounding mantle. However, seismic studies detected the existence of 3%–5% low compressional-wave velocity anomalies accompanied with strong seismic shear-wave anisotropies within the subducting slab at the top transition zone in various locations of the Earth which cannot be explained by the presence of metastable olivine alone. Besides olivine, orthopyroxene could also remain metastable in the coldest harzburgite layer of the slab. Here we report experimental results on the single-crystal elasticity of both α- and β-orthopyroxene up to 20 GPa and 300 K. These experimental results allow us to provide a comprehensive evaluation on the velocity profiles of the coldest harzburgite layer of the slab. We found that the coldest harzburgite layer with 22–37 vol.% orthopyroxene and 62–78 vol.% olivine has the V_P and V_S 3.0%–4.4(6)% and 2.0%–4.5(6)% lower than those of the pyrolitic mantle in the mantle transition zone, respectively. The observed 3%–5% low-velocity anomalies within the slab in the top transition zone should be explained by the metastable orthopyroxene and olivine instead of metastable olivine alone.

1. Introduction

Seismic studies suggested the existence of 3%–5% low compressional-wave velocity (V_P) anomalies with strong shear-wave (V_S) splitting within sinking subduction slabs at 410 to 520-km depths of the mantle transition zone (Jiang et al., 2008; Kaneshima et al., 2007; Liu et al., 2008; Pankow et al., 2002; Tono et al., 2009). These observed velocity anomalies were previously proposed to be related to the existence of metastable wedge, because the velocity of metastable olivine is a few percent lower than its high-pressure polymorphs at the transition zone depths (Mao et al., 2015). The observed V_S-splitting could be explained by the deformation of the olivine wedge when its volume percentage is over 40% (Bernard et al., 2021; Kirby et al., 1996; Mao et al., 2015; Mosenfelder et al., 2001; Raterron et al., 2002). Besides olivine, orthopyroxene is one of the major constituent minerals in the harzburgite layer of the sinking slab and could also remain metastable at the transition zone depth within the cold slab which is 700–1000 K colder than the surrounding mantle (Ganguly et al., 2009; King et al., 2015; Nishi et al., 2013; Van Mierlo et al., 2013). However, the contribution of metastable orthopyroxene

Writing – review & editing: Luo Li, Ningyu Sun, Weigang Shi, Zhu Mao, Yingxin Yu, Yanyao Zhang, Jung-Fu Lin

to the velocity profiles of the coldest harzburgite layer has not been considered, and knowledge about the elasticity of the high-pressure orthopyroxene phases is thus key to decipher the formation mechanism of the observed low-velocity anomalies within the cold slabs.

Under ambient conditions, orthopyroxene crystallizes in an orthorhombic structure with the space group of *Pbca* (α-orthopyroxene) (Cameron & Papike, 1981). The elasticity of α-orthopyroxene at ambient conditions has been extensively studied using various experimental techniques (Angel & Jackson, 2002; Bass & Weidner, 1984; Chai et al., 1997; Duffy & Vaughan, 1988; Jackson et al., 1999; Kumazawa, 1969; Webb & Jackson, 1993; Weidner & Vaughan, 1982; Weidner et al., 1978; Zhang & Bass, 2016). Elevating the temperature at ambient conditions was observed to cause a linear decrease in all elastic moduli (Hogrefe et al., 1994; Jackson et al., 2004, 2007; Reynard et al., 2010; Zhao et al., 1995). Along a slab geotherm that is 700–1000 K colder than the surrounding mantle, metastable α-orthopyroxene in the harzburgite layer of the sinking slab will transform into the monoclinic β-phase ($P2_1/c$ space group) with a Clapeyron slope of −8.9 to 20 MPa/K which could be carried down to 500-km depth (Lin, 2004; Xu et al., 2018, 2022; J. S. Zhang et al., 2012, 2014). However, experimental constraints on the elasticity of β-phase at high pressures are rather limited, and the influence of the α- to β-phase transition on the elasticity of orthopyroxene is still under debate (Kung et al., 2004; Zhang & Bass, 2016; D. Zhang et al., 2013).

A previous Brillouin study has shown that the α- to β-phase transition at 12 GPa and 300 K can cause a ∼1% jump in both compressional (V_P) and shear-wave (V_S) velocities (Zhang & Bass, 2016). However, this conclusion heavily relied on one experimental data point for the elasticity of the β-phase, and the pressure dependence on the elasticity of the β-phase could not be constrained (Zhang & Bass, 2016). In contrast, ultrasonic measurements observed a strong softening in the V_P and V_S across the phase transition, indicating that the presence of β-orthopyroxene could also be responsible for the origin of the low V_P anomalies within the subducting slab instead of the metastable olivine alone (Kung et al., 2004). In addition, nuclear resonant inelastic X-ray scattering (NRIXS) measurements reported similar softening in the V_S but no anomalous change was detected in the V_P across the α- to β-phase transition (Kung et al., 2004; D. Zhang et al., 2013). High-pressure studies on the elasticity of orthopyroxene across this phase transition are thus needed to resolve the conflicting results in previous studies.

In this study, we have determined the full elastic moduli (C_{ij}) of single-crystal Fe-bearing orthopyroxene using Brillouin scattering in short symmetric diamond anvil cells (DACs) up to 20 GPa. The results are used to constrain the velocity profiles of both α- and β-orthopyroxene at high pressures. Together with literature results, we have modeled the density and velocity profiles of the coldest harzburgite layer of the subduction slab with metastable orthopyroxene and olivine. These results provide additional information into understanding the origin of the observed low-velocity anomalies within the cold subduction slab.

2. Experiment

Natural single-crystal orthopyroxene from Yangon, Myanmar was analyzed for its composition using an electron microprobe in the Key Laboratory of Crust-Mantle Materials and Environments, University of Science and Technology of China (USTC). The analysis yielded a composition of $Mg_{0.86}Fe_{0.11}Al_{0.02}Ca_{0.01}Si_{0.99}O_3$ on the oxides basis. The density of 3.329(4) g/cm^3 with an orthorhombic structure at ambient conditions was determined by single-crystal X-ray diffraction at beamline 15U, Shanghai Synchrotron Radiation Facility. We chose one platelet of plane (010) based on the crystal cleavage. Other two sample platelets were cut from the same crystal perpendicular to the (010) platelet, and the two platelets are orthogonal to each other. Three platelets of ∼100 μm in diameter were double-side polished to ∼25 μm in thickness and loaded into the sample chamber of the DAC equipped with a pair of 400 or 500-μm culet diamonds and Re as the gasket material. Two ruby spheres were loaded into the sample chamber as the pressure calibrant, and argon was used as the pressure medium for high pressure experiments (Dewaele et al., 2004). The deviatoric stress inside the DAC using Ar as the pressure medium was evaluated using the variations of the XRD peaks of Pt. We found that the deviatoric stress is 0.011(2) at 10.0 GPa and 0.011(3) at 15.4 GPa (Singh, 1993).

High pressure Brillouin measurements on the crystal platelets were conducted at the High-Pressure Mineral Physics Laboratory, USTC up to 20 GPa at 300 K (Figure S4 in Supporting Information S1). Experiments were performed in a forward scattering geometry using a six-pass Sandercock tandem Fabry-Perot interferometer.

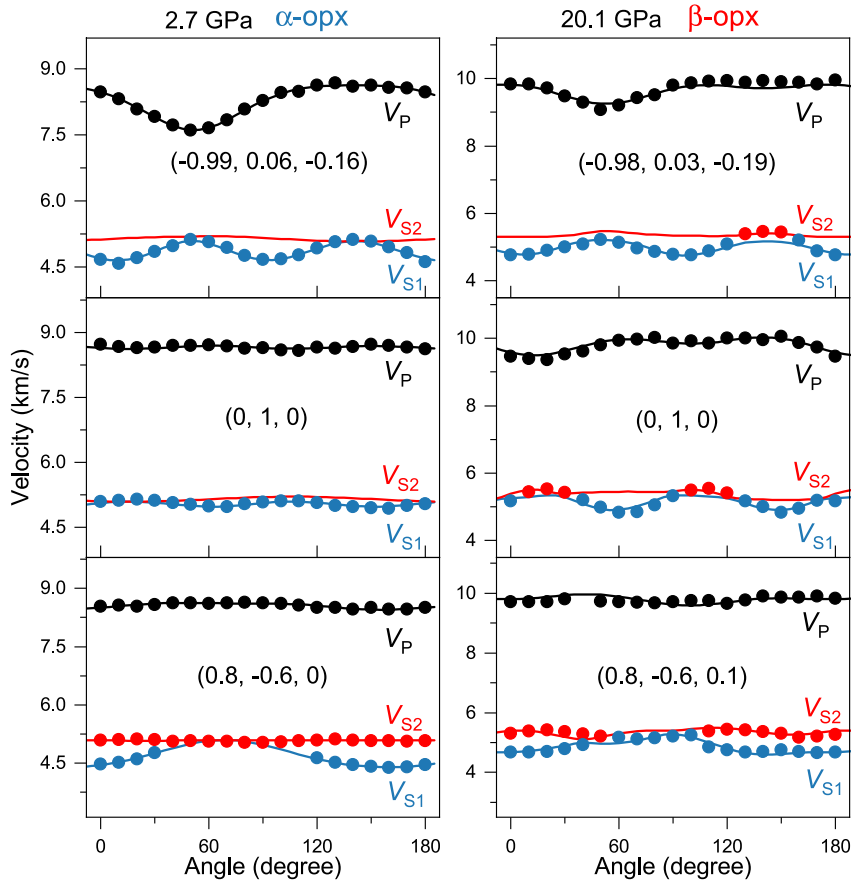

Figure 1. Representative acoustic velocities of orthopyroxene measured at 2.7 and 20.1 GPa as a function of azimuthal angles. Circles: measured velocities; lines: fitting results; black: quasi-longitudinal modes; red: fast quasi-shear mode; blue: slow quasi-shear mode. The orientations of each crystal platelet are shown in the figure.

The acoustic velocities of the orthopyroxene platelet along a specific direction were derived from the measured Brillouin frequency shift as follows:

$$v = \frac{\Delta v_B \lambda_0}{2\sin(\theta/2)} \quad (1)$$

where v is the acoustic velocity, Δv_B is the measured Brillouin frequency shift, λ_0 is the laser wavelength (532 nm), and θ is the external scattering angle (49.3°). Due to the low-symmetry of orthopyroxene, there are 9 independent elastic moduli for the α-phase and 13 moduli for the β-phase. For each platelet at a given pressure, we thus measured the sound velocities of orthopyroxene at 10° steps in a total of 19 directions over a range of 180° (Figure 1). In total, the different crystallographic directions from 0 to 180° of the V_P, V_{S1}, and V_{S2} velocity data were used to derive the full elastic moduli (C_{ij}) of the single crystal at each given pressure.

In situ Raman and single-crystal XRD measurements were also conducted to confirm the crystalline phase of the platelets in short symmetric DACs at the High-Pressure Mineral Physics Laboratory, USTC and the 13-ID-D experimental station of the Advanced Photon Source, Argonne National Laboratory, respectively. An Olympus flat field achromatic objective lens was employed for the collection of Raman spectra with a 532 nm wavelength laser line. The Raman spectra were measured in a backscattering geometry in a confocal configuration. We have performed two runs of Raman measurements. The Raman spectra were collected every 0.1–1.7 GPa up to 20 GPa at 300 K (Figures S1 and S2 in Supporting Information S1). High-quality diffraction images of the orthopyroxene were analyzed to determine the unit-cell parameters before and after phase transition with the known structures (Figure S3 in Supporting Information S1). The obtained the lattice parameters for α-orthopyroxene

are a = 18.0334(8) Å, b = 8.5630(5) Å, c = 5.0621(5) Å at 10.0 GPa, while a, b, c, and β for the beta-phase are 17.839(1), 8.556(1), 4.9376(3), and 92.873(5) Å at 15.4 GPa, respectively.

3. Results

Analysis of the Raman spectra shows that α-orthopyroxene can be confidently identified using the observed 25 active Raman modes at ambient conditions and at pressures (Figures S1 and S2 in Supporting Information S1). The frequency of all the Raman modes in α-orthopyroxene followed a nearly linear increase with pressure up to 15 GPa. At pressures above 15 GPa, 11 new Raman modes were present, and 6 modes belonging to the α-phase disappeared. The XRD results indicated that the orthopyroxene crystal underwent pseudomerohedral twinning and developed two twin domains connected by the (001) twinning mirror plane after transitioning into the β-phase (Dera et al., 2013; Finkelstein et al., 2015). Since all three platelets used in our Brillouin measurements are nearly perpendicular to the X-Y plane, the influence of twinning is minimal on our Brillouin measurements.

The single-crystal elastic compliances of orthopyroxene were calculated by fitting the measured acoustic velocities using the Christoffel equation (Brown, 2018; Brown et al., 1989; Every, 1980) (Figures 1 and 2, Figure S11 and Table S1 in Supporting Information S1):

$$|C_{ijkl}n_j n_l - \rho v^2 \delta_{ik}| = 0 \quad (2)$$

where C_{ijkl} is the elastic tensor (with the full suffix notation of the elastic matrix), n_j and n_l are the direction cosines in the photon propagation direction calculated by the azimuthal angles of different platelets, respectively, ρ is density, ν is the acoustic velocity, and δ_{ik} is the Kronecker delta function. The orientations of each platelet were determined by an iterative inversion process (Text S1 in Supporting Information S1). For α-orthopyroxene, ρ at high pressures was determined following a self-consistent procedure using the Brillouin data (Speziale & Duffy, 2002). At ambient conditions, the bulk (K_{S0}) and shear (G_0) moduli of α-orthopyroxene calculated from the single-crystal elasticity were 107.8(7) and 77.1(6) GPa, respectively (Figure 2). Analysis of the sensitivity of the crystal orientations between each C_{ij}, the direction-dependent velocities (V_P, V_{S1}, and V_{S2}), and the number of measured phonon directions show that the crystal orientations in this study are appropriate for constraining all C_{ij}s in Figure S7 in Supporting Information S1.

Analysis of the derived elastic results shows an obvious softening in the shear waves in third platelet with azimuthal angles of 10°, 20°, and 30° between 10 and 15 GPa (Figure S5 in Supporting Information S1). Together with the Raman and SCXRD results, we determined the phase transition from the α- to β-phase to be at 15 GPa and 300 K (Figures S2 and S3 in Supporting Information S1). For α-orthopyroxene with an orthorhombic structure, all the shear moduli C_{44}, C_{55}, and C_{66} exhibit an obvious softening starting from 10 GPa (Figures 2a and 2b). The third- or fourth-order finite equations were used to fit all the C_{ij}s for α-orthopyroxene. We considered a 2.3(1)% jump in density across the α- to β-phase using literature results (Figure S8 in Supporting Information S1) (Dera et al., 2013; Finkelstein et al., 2015; Xu et al., 2018, 2020, 2022; Zhang & Bass, 2016; D. Zhang et al., 2013; J. S. Zhang et al., 2012). The density of the β-phase between 15 and 20 GPa was also derived following the self-consistent procedure using the Brillouin data (Sata et al., 2002). All the 13 single-crystal elastic moduli of the β-phase exhibit a linear dependence on pressure up to 20 GPa. An increase in C_{22}, C_{44}, C_{55}, and C_{23} as well as an apparent drop in C_{66} occur across the α- to β-phase transition. Other moduli show a change in the pressure dependence across this phase transition. The values of the C_{15}, C_{25}, C_{35}, and C_{46} elastic moduli of the monoclinic β-phase are small (close to zero) compared to other elastic moduli. In particular, both C_{35} and C_{46} are negative and slightly decrease with increasing pressure. We note that negative elastic moduli have been reported for similar monoclinic silicates and oxides, such as diopside, chondrodite, and epidote (Bass, 1995; Sang & Bass, 2014; Sinogeikin & Bass, 1999).

4. Discussion

Our orthopyroxene contains 11 mol.% Fe, and the obtained results was first used to understand the influence of Fe on the density and elastic moduli of α-orthopyroxene at ambient conditions (Figure S9 and Table S3 in Supporting Information S1). Here, we focus on the density and elasticity of orthopyroxene along the enstatite-ferrosilite join while ignoring the influence of Al. These analyses show that increasing the Fe content leads to a linear decrease in both K_{S0} and G_0 of α-orthopyroxene but results in an linear increase in density (Angel & Jackson, 2002;

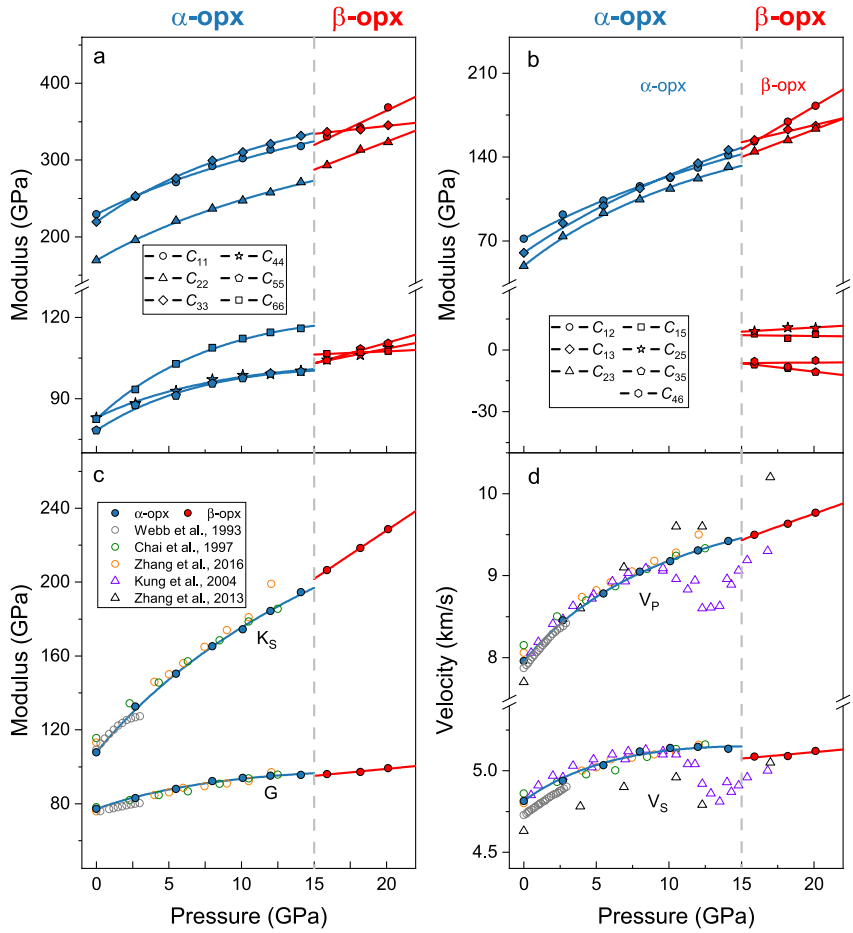

Figure 2. Single-crystal elasticity orthopyroxene at high pressures and 300 K. Blue: α-orthopyroxene in this study; red: β-orthopyroxene in this study. (a) Longitudinal and shear moduli. Circles: C_{11}; triangles: C_{22}; diamonds: C_{33}; stars: C_{44}; pentagons: C_{55}; squares: C_{66}; blue lines: the fitting results of α-orthopyroxene; red lines: the fitting results of β-orthopyroxene; (b) Off-diagonal moduli. Circles: C_{12}; diamonds: C_{13}; triangles: C_{23}; squares: C_{15}; stars: C_{25}; pentagons: C_{35}; hexagons: C_{46}; blue lines: the fitting results of α-orthopyroxene; red lines: the fitting results of β-orthopyroxene; (c) K_S and G. (d) V_P and V_S of orthopyroxene. Gray circles: Webb & Jackson, 1993; green circles: Chai et al., 1997; orange circles: Zhang & Bass, 2016; blue lines: the fitting results of α-orthopyroxene; red lines: the fitting results of β-orthopyroxene; open circles; Purple (Kung et al., 2004) and black (D. Zhang et al., 2013) open triangles; blue lines: the fitting results of α-orthopyroxene; red lines: the fitting results of β-orthopyroxene.

HughJones et al., 1996; Jackson et al., 2007; Webb & Jackson, 1993; Zhang & Bass, 2016). Addition of Fe was noted to have a stronger effect on G_0 than K_{S0}. The substitution of 10 mol. % Mg by Fe lowers the G_0 by 3.3(5)% but could only cause a 1.1(2)% reduction in the K_{S0}. The addition of 10 mol.% could increase the density of α-orthopyroxene by 2.9(4)%.

Combining our Raman and Brillouin measurements, the α- to β-phase transition in orthopyroxene was determined to occur at 15 GPa (Figures S1, S2, and S5 in Supporting Information S1). We also analyzed the velocity data using the orthorhombic structure for the β-phase. However, there are several apparent misfits when fitting the measured velocities using the orthorhombic structure, and the root-mean-square (RMS) is 130 m/s which is much greater than RMS of 80 m/s by using the monoclinic structure for the β-phase (Figure S10 in Supporting Information S1). For α-orthopyroxene, all the C_{ij}s at high pressures are in good agreement with previous single-crystal experimental results, although the longitudinal modulus, C_{11}, is slightly lower than literature results, whereas shear moduli, C_{55} and C_{66}, are greater (Figures 2a and 2b) (Chai et al., 1997; Webb & Jackson, 1993; Zhang & Bass, 2016). The only single-crystal elasticity data for the β-phase before this study is from Zhang and Bass (2016), although they have only one elasticity data point for the β-phase. A sudden increase in all longitudinal moduli except C_{55} was observed across the α- to β-phase transition (Zhang & Bass, 2016).

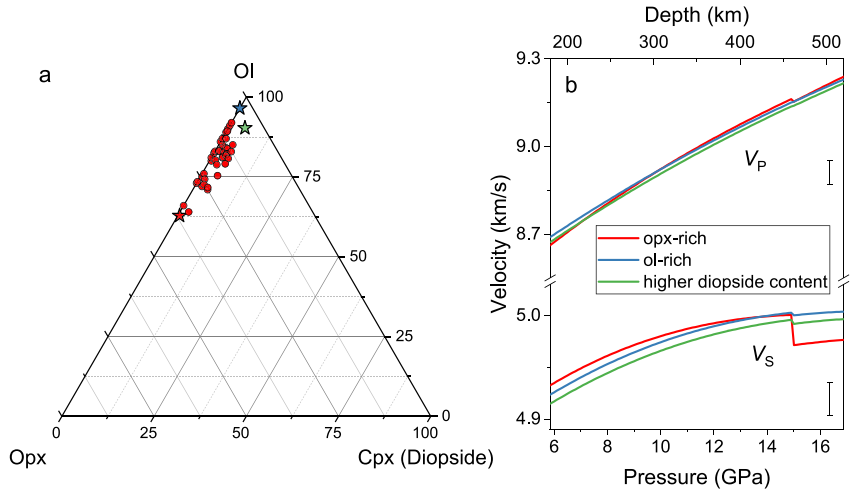

Figure 3. Depth-dependent velocity profiles of harzburgite with three distinct mineral contents of olivine, orthopyroxene, and clinopyroxene. (a) Composition of harzburgite (Downes et al., 1992; Foley et al., 2006; Furnes et al., 1986; Raye et al., 2011); Ol: olivine; Opx: orthopyroxene; Cpx: clinopyroxene-diopside; red circles: composition of harzburgite layer obtained by previous petrological observations; red, blue, and green stars indicate the composition of harzburgite used in velocity modelings in panel (b); (b) Velocity of the coldest harzburgite layer along a slab geotherm 1000 K colder than the normal mantle in three selected composition highlight in red, blue, and green stars in panel (a) (Ganguly et al., 2009). Red lines: velocity of harzburgite with 37 vol.% orthopyroxene, 62.5 vol.% olivine, and 0.5 vol.% clinopyroxene; blue lines: velocity of harzburgite with 3.5 vol.% orthopyroxene and 96.5 vol.% olivine; green lines: velocity of harzburgite with 5 vol.% orthopyroxene, 90 vol.% olivine, and 5 vol.% clinopyroxene. Model uncertainties are shown as vertical ticks on the right.

Here, we analyzed the single-crystal elasticity of the β-phase using the monoclinic structure (Dera et al., 2013; J. S. Zhang et al., 2012). We only observed a sudden weak increase in C_{22}, C_{44}, C_{55}, and C_{23} accompanied with a drop in the value of C_{66} across this phase transition, and other elastic moduli exhibit a change in the pressure dependence, which is in contrast to previous Brillouin results (Zhang & Bass, 2016).

Using the obtained single-crystal elastic moduli and density, we calculated the aggregate K_S, G, and the sound velocities for both α- and β-phase (Figures 2c and 2d). Our calculated results have shown that the α- to β-phase transition leads to a 5.8(6)% sudden jump in the K_S but a 3.7(5)% drop in G. Together with the density change, the transition from the α- to β-phase can produce a 1.6(5)% sudden drop in V_S at 300 K which is much less than the strong softening reported in previous NRIXS and ultrasonic measurements (Kung et al., 2004; J. S. Zhang et al., 2012). The major influence of this phase transition on V_P is the change in the pressure dependence. This is also in contrast to the strong softening in V_P shown in the ultrasonic measurements but in a general agreement with the NRIXS measurements, although the value of V_P from the NRIXS study for both α- and β-phase is much greater than our measured results (Kung et al., 2004; J. S. Zhang et al., 2012). As we noted above, the measured V_S along a few azimuthal angles between 10 and 15 GPa exhibit strong softening (Figure S5 in Supporting Information S1). The polycrystalline orthopyroxene used in previous ultrasonic and NRIXS experiments may have developed a certain degree of lattice preferred orientation across the α- to β-phase transition (Kung et al., 2004; D. Zhang et al., 2013), which in turn could influence the reported elasticity results and cause the differences between this study and previous reports.

5. Geophysical Implications

To investigate the origin of the low-velocity anomalies inside the sinking subduction slab, here we have modeled the velocity profiles of the coldest subducting harzburgite layer along a slab geotherm 1000-K lower than the normal mantle (Brudzinski & Chen, 2000, 2003; Chen & Brudzinski, 2003; Kaneshima et al., 2007). Harzburgite is mainly composed of olivine and orthopyroxene with a small amount of clinopyroxene, whereas the volume ratio between olivine and pyroxene can exhibit a wide compositional range based on previous petrological observations (Figure 3) (Downes et al., 1992; Foley et al., 2006; Furnes et al., 1986; Raye et al., 2011). We first calculated the V_P and V_S of orthopyroxene, olivine, and clinopyroxene along a 1000-K colder slab geotherm (Collins & Brown, 1998; Jackson et al., 2003; Li & Neuville, 2010; Liu & Li, 2006; Mao et al., 2015; Zhao et al., 1995). Due

to lack experimental constraints, here we considered the same temperature derivative of the elastic moduli for the β-phase as α-orthopyroxene (Table S4 in Supporting Information S1) (Jackson et al., 2003; Zhao et al., 1995). Literature results on the influence of temperature on the phase transition pressure of orthopyroxene were applied in our modeling (Table S5 in Supporting Information S1) (Xu et al., 2018, 2020; J. S. Zhang et al., 2014). In such a cold subduction environment, olivine will remain in the metastable phase up to 520-km depth in the mantle transition zone, and α-orthopyroxene transforms into the β-phase at depth of 460 km (Ishii & Ohtani, 2021; Kawakatsu & Yoshioka, 2011; Lidaka & Suetsugu, 1992; Xu et al., 2018, 2020).

Along the 1000-K colder slab geotherm, the difference in V_P (V_S) between α-orthopyroxene and olivine is less than 0.6(4)% (0.7(5)%) up to the depth of 450 km, which is negligible by considering the calculation uncertainties (Figure S12 in Supporting Information S1) (Liu & Li, 2006; Mao et al., 2015). The transition from α-orthopyroxene to the β-phase was noted to cause a 1.6(5)% sudden reduction in the V_S but has a weak influence on the V_P. Above 460-km depth, V_S of the β-phase is 1.6(5)% lower than that of olivine, while the difference in V_P is less than 0.2(5)%. Both olivine and α-orthopyroxene have sound velocities greater than clinopyroxene up to 520-km depth. For a multiphase assemblage, the density and elastic moduli were calculated using the following equations (Cottaar et al., 2014):

$$\rho = \sum \rho_i V_i \tag{3}$$

$$M = \frac{1}{2}\left[\sum V_i M_i + \left(\sum V_i M_i^{-1}\right)^{-1}\right] \tag{4}$$

where ρ_i, V_i, and M_i are the density, volume percentage, and elastic moduli (K_S and G) of the ith phase, respectively. Here, K_S and G were calculated within the Voigt-Reuss-Hill average scheme. V_P and V_S of a multiphase assemblage were calculated as follows:

$$V_P = \sqrt{\frac{K_S + 4G/3}{\rho}} \tag{5}$$

$$V_S = \sqrt{\frac{G}{\rho}} \tag{6}$$

where K_S is the adiabatic bulk modulus, and G is the shear modulus. Considering how the variations in composition may influence the velocity of harzburgite in the subducting slab, we calculated the velocities of harzburgite in three different compositions: (a) olivine rich model with 3.5 vol.% orthopyroxene and 96.5 vol.% olivine; (b) orthopyroxene rich model with 37 vol.% orthopyroxene, 62.5 vol.% olivine, and 0.5 vol.% diopside; (c) higher clinopyroxene (diopside) content model with 5 vol.% orthopyroxene, 90 vol.% olivine, and 5 vol.% diopside (Figure 3). Considering the calculation uncertainties, varying the composition of harzburgite has minimal effect on its velocities up to 460-km depth. Due to a different orthopyroxene content, elevating the orthopyroxene content to 37 vol.% can lead to a maximum of 0.6(5)% reduction in the V_S but can hardly affect the V_P considering the calculation errors. As a result, harzburgite with 37 vol.% β-orthopyroxene at 460–520 km depth has the V_S 0.5(5)% lower than that with 3.5 vol.% β-phase.

We further examined the seismic signature of the coldest harzburgite layer with or without considering the contribution of metastable orthopyroxene. The velocities of subducted mid-ocean ridge basalts (MORBs), the lherzolite layer of the sinking slab, and the pyrolitic mantle were also calculated for comparison (Table S4 and Figure S13 in Supporting Information S1). The temperature of MORBs was assumed to be the same as that of the surrounding pyrolitic mantle (Brown & Shankland, 1981), while the velocity profiles of the lherzolite layer with 65 vol.% olivine, 20 vol.% orthopyroxene and 15 vol.% clinopyroxene is modeled with a temperature profile of 600 K lower than that of the pyrolitic mantle (Ganguly et al., 2009; Ringwood & Irifune, 1988). Here, we adopted a typical harzburgite composition from Tamura and Arai (2006) with 22 vol.% orthopyroxene and 78 vol.% olivine (Tamura & Arai, 2006). Our modeled velocity profiles here show that the coldest harzburgite layer in the upper mantle up to 340-km depth with metastable orthopyroxene and olivine has the fastest V_P and V_S compared to the MORBs, underlying lherzolite, and the pyrolitic mantle due to its lower temperature profile (Figure 4). The V_P of harzburgite is 3.0%–4.4(6)% greater than that of MORBs, lherzolite, and the pyrolitic mantle at 250-km depth, while its V_S is 3.8%–6.2(6)% faster. Increasing depth can greatly reduce the velocity difference between the

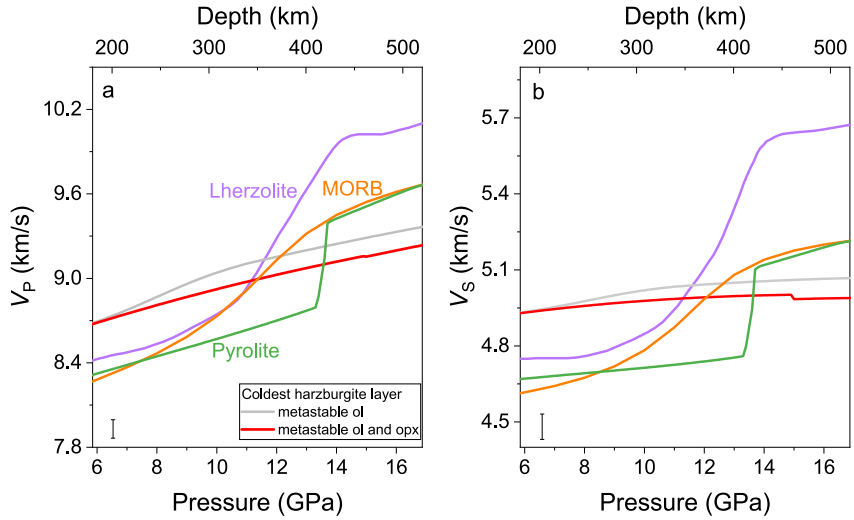

Figure 4. Velocity of coldest harzburgite layer, lherzolite, mid-ocean ridge basalts (MORBs), and pyrolitic mantle. (a) Compressional wave velocity (V_P); (b) shear-wave velocity (V_S). Red lines: harzburgite with 22 vol.% orthopyroxene and 78 vol.% olivine. Both orthopyroxene and olivine remain metastable up to 520-km depth; purple lines: velocity of lherzolite with 65 vol.% olivine, 20 vol.% orthopyroxene, and 15 vol.% clinopyroxene; orange lines: velocity of MORBs; green lines: velocity of the pyrolitic mantle. Model uncertainties are shown as vertical ticks on the left.

coldest harzburgite layer and MORBs as well as lherzolite, because the phase transition from coesite to stishovite and from olivine to its high-pressure polymorphs can effectively increase the velocity of MORB and lherzolite, respectively (Akimoto & Syono, 1969; Katsura et al., 2004; Schutt & Lesher, 2006; J. Zhang et al., 1996). The velocity crossover between harzburgite and MORBs (lherzolite) occurs at 350-km (340-km) depth. Above 350-km depth, the coldest harzburgite layer with low-velocity olivine and orthopyroxene becomes the slowest part of the sinking slab but has the sound velocity still faster than that of the pyrolitic mantle.

At 410-km depth, both MORBs and lherzolite have sound velocities indistinguishable from or faster than the pyrolitic mantle (Figure 4). The coldest harzburgite layer begins to display slower velocities than the pyrolitic mantle because the phase transition from olivine to wadsleyite in the normal mantle can cause a 4%–5% sudden jump in the V_P and V_S, whereas both olivine and orthopyroxene in harzburgite remain in the metastable phases (Dera et al., 2013; Hogrefe et al., 1994; Kaneshima et al., 2007; Mao et al., 2015). If we ignore the contribution of metastable orthopyroxene but only consider metastable olivine in the coldest harzburgite layer below 410-km depth, metastable olivine should coexist with the high-velocity garnet and high-pressure clinopyroxene in the harzburgite layer at this depth range (Irifune & Ringwood, 1987). As a result, V_P and V_S of harzburgite are only 2.3(6)% and 1.7(6)% lower than those of the pyrolitic mantle, respectively, which is not enough to interpret the observed 3%–5% low V_P anomalies within the slab (Kaneshima et al., 2007; Lidaka & Suetsugu, 1992; Mao et al., 2015). Unless the olivine content in harzburgite is as large as 96 vol.%, this metastable wedge could have the V_P 3%–4% lower than the pyrolitic mantle between 410 and 520-km depth (Figure S13 in Supporting Information S1).

With considering the contribution of metastable orthopyroxene, V_P of the coldest harzburgite layer is 3.0%–3.6(6)% lower than that of pyrolitic mantle between 410 and 460-km depth, and V_S is 2.0%–2.9(6)% lower (Figure 4). The α- to β-phase transition in orthopyroxene along the 1000-K colder slab geotherm can further lower the V_S of harzburgite but has a minimal effect on the V_P. More importantly, both V_P and V_S of harzburgite with metastable olivine and β-orthopyroxene exhibit weaker pressure (depth) dependence than those of the pyrolitic mantle, and their difference in velocity thus increases with depth (Figure 4). As a result, the coldest harzburgite layer with the metastable β-orthopyroxene and olivine has the V_P 3.6%–4.4(6)% less than the pyrolitic mantle at 460–520-km depth, better consistent with the observed 3%–5% low V_P anomalies within the sinking slabs (Jiang et al., 2008; Kaneshima et al., 2007; Liu et al., 2008; Pankow et al., 2002; Tono et al., 2009). Meanwhile, this metastable wedge with both orthopyroxene and olivine has the V_S 2.8%–4.3(6)% lower than the surrounding mantle. Increasing the orthopyroxene content to 37 vol.% can generate a harzburgite layer with 2.9%–4.5(6)% lower V_S than the pyrolitic mantle at 460–520 km depth but has a minimal effect on the V_P, because the difference in the V_P between

metastable olivine and β-orthopyroxene is small (Figures S13 in Supporting Information S1). We thus propose that the observed 3%–5% low-velocity anomalies in the mantle transition between 410 and 520-km depth within the sinking slabs should be caused by the presence of metastable olivine, α- and β-phase orthopyroxene instead of metastable olivine alone (Jiang et al., 2008; Kaneshima et al., 2007; Liu et al., 2008; Pankow et al., 2002; Tono et al., 2009).

In summary, we have determined the single-crystal elasticity of α- and β-orthopyroxene at high pressures up to 20 GPa at 300 K by combining Brillouin and Raman spectroscopies. At 300 K, the α- to β-phase transition occurs at 15 GPa and produces an obvious change in all the single-crystal elastic moduli. Together with literature results, we have established the velocity profiles of the coldest harzburgite layer within the sinking slab with metastable orthopyroxene and olivine as the major constituent phases up to 520-km depth. The coldest harzburgite layer with 22–37 vol.% orthopyroxene and 62–78 vol.% olivine has the V_P and V_S 3.0%–4.4(6)% and 2.0%–4.5(6)% lower than those of the pyrolitic mantle in the mantle transition zone, respectively. Considering the contribution from both metastable orthopyroxene and olivine, the seismic signature of the coldest harzburgite layer is in a better agreement with the observed 3%–5% low V_P anomalies within the sinking slab in various locations of the Earth at depth of 410–520 km in the mantle transition zone. The low-velocity metastable wedge within the sinking slab should thus be composed by orthopyroxene and olivine instead of metastable olivine alone.

Conflict of Interest

The authors declare no conflicts of interest relevant to this study.

Data Availability Statement

Experimental data for Figures 1 and 2 are listed in Tables S1–S3 in Supporting Information S1. A more detailed information of the experimental results is also available in the supplementary material. All the reference data are listed in Tables S4 and S5 in Supporting Information S1. They can also be downloaded online (https://zenodo.org/record/6477209).

Acknowledgments
This work is supported by the B-type Strategic Priority Program of the Chinese Academy of Sciences (Grant No. XDB41000000), China National Science Foundation (41590621), and the Fundamental Research Funds for the Central Universities (WK2080000144). XRD data was collected at BL15U1 of Shanghai Synchrotron Radiation Facility (proposal 2019-SSRF-PT-011379) and 13-ID-D of the Advanced Photon Source, Argonne National Laboratory (proposal 2022-GUP-ID-71124). JFL acknowledges support from the Geophysics Program of the National Science Foundation, USA (EAR-1916941).

References

Akimoto, S.-I., & Syono, Y. (1969). Coesite-Stishovite transition. *Journal of Geophysical Research*, *74*(6), 1653–1659. https://doi.org/10.1029/JB074i006p01653

Angel, R. J., & Jackson, J. M. (2002). Elasticity and equation of state of orthoenstatite. $MgSiO_3$, *American Mineralogist*, *87*(4), 558–561. https://doi.org/10.2138/am-2002-0419

Bass, J. D. (1995). Elasticity of minerals, glasses, and melts. In *Mineral Physics & Crystallography* (Vol. 2, pp. 45–63). https://doi.org/10.1029/RF002p0045

Bass, J. D., & Weidner, D. J. (1984). Elasticity of single-crystal orthoferrosilite. *Journal of Geophysical Research*, *89*(B6), 4359–4371. https://doi.org/10.1029/JB089iB06p04359

Bernard, R. E., Schulte-Pelkum, V., & Behr, W. M. (2021). The competing effects of olivine and orthopyroxene CPO on seismic anisotropy. *Tectonophysics*, *814*, 228954. https://doi.org/10.1016/j.tecto.2021.228954

Brown, J., Slutsky, L., Nelson, K., & Cheng, L. T. (1989). Single-crystal elastic constants for San Carlos peridot: An application of impulsive stimulated scattering. *Journal of Geophysical Research*, *94*(B7), 9485–9492. https://doi.org/10.1029/jb094ib07p09485

Brown, J. M. (2018). Determination of elastic moduli from measured acoustic velocities. *Ultrasonics*, *90*, 23–31. https://doi.org/10.1016/j.ultras.2018.05.015

Brown, J. M., & Shankland, T. J. (1981). Thermodynamic parameters in the Earth as determined from seismic profiles. *Geophysical Journal International*, *66*(3), 579–596. https://doi.org/10.1111/j.1365-246X.1981.tb04891.x

Brudzinski, M. R., & Chen, W. P. (2000). Variations in P wave speeds and outboard earthquakes: Evidence for a petrologic anomaly in the mantle transition zone. *Journal of Geophysical Research*, *105*(B9), 21661–21682. https://doi.org/10.1029/2000jb900160

Brudzinski, M. R., & Chen, W. P. (2003). A petrologic anomaly accompanying outboard earthquakes beneath Fiji-Tonga: Corresponding evidence from broadband P and S waveforms. *Journal of Geophysical Research*, *108*(B6), 19. https://doi.org/10.1029/2002jb002012

Cameron, M., & Papike, J. J. (1981). Structural and chemical variations in pyroxenes. *American Mineralogist*, *66*(1–2), 1–50.

Chai, M., Brown, J. M., & Slutsky, L. J. (1997). The elastic constants of an aluminous orthopyroxene to 12.5 GPa. *Journal of Geophysical Research*, *102*(B7), 14779–14785. https://doi.org/10.1029/97jb00893

Chen, W. P., & Brudzinski, M. R. (2003). Seismic anisotropy in the mantle transition zone beneath Fiji-Tonga. *Geophysical Research Letters*, *30*(13), 4. https://doi.org/10.1029/2002gl016330

Collins, M. D., & Brown, J. M. (1998). Elasticity of an upper mantle clinopyroxene. *Physics and Chemistry of Minerals*, *26*(1), 7–13. https://doi.org/10.1007/s002690050156

Cottaar, S., Heister, T., Rose, I., & Unterborn, C. (2014). BurnMan: A lower mantle mineral physics toolkit. *Geochemistry, Geophysics, Geosystems*, *15*(4), 1164–1179. https://doi.org/10.1002/2013gc005122

Dera, P., Finkelstein, G. J., Duffy, T. S., Downs, R. T., Meng, Y., Prakapenka, V., & Tkachev, S. (2013). Metastable high-pressure transformations of orthoferrosilite Fs(82). *Physics of the Earth and Planetary Interiors*, *221*, 15–21. https://doi.org/10.1016/j.pepi.2013.06.006

Dewaele, A., Loubeyre, P., & Mezouar, M. (2004). Equations of state of six metals above 94 GPa. *Physical Review B*, *70*(9), 094112. https://doi.org/10.1103/physrevb.70.094112

Downes, H., Embey-Isztin, A., & Thirlwall, M. F. (1992). Petrology and geochemistry of spinel peridotite xenoliths from the western Pannonian Basin (Hungary): Evidence for an association between enrichment and texture in the upper mantle. *Contributions to Mineralogy and Petrology*, *109*(3), 340–354. https://doi.org/10.1007/BF00283323

Duffy, T. S., & Vaughan, M. T. (1988). Elasticity of enstatite and its relationship to crystal structure. *Journal of Geophysical Research*, *93*(B1), 383–391. https://doi.org/10.1029/JB093iB01p00383

Every, A. G. (1980). General closed-form expressions for acoustic waves in elastically anisotropic solids. *Physical Review B*, *22*(4), 1746–1760. https://doi.org/10.1103/PhysRevB.22.1746

Finkelstein, G. J., Dera, P. K., & Duffy, T. S. (2015). Phase transitions in orthopyroxene (En_{90}) to 49 GPa from single-crystal X-ray diffraction. *Physics of the Earth and Planetary Interiors*, *244*, 78–86. https://doi.org/10.1016/j.pepi.2014.10.009

Foley, S. F., Andronikov, A. V., Jacob, D. E., & Melzer, S. (2006). Evidence from Antarctic mantle peridotite xenoliths for changes in mineralogy, geochemistry and geothermal gradients beneath a developing rift. *Geochimica et Cosmochimica Acta*, *70*(12), 3096–3120. https://doi.org/10.1016/j.gca.2006.03.010

Furnes, H., Pedersen, R. B., & Maaloe, S. (1986). Petrology and geochemistry of spinel peridotite nodules and host basalt, Vestspitsbergen. *Norsk Geologisk Tidsskrift*, *66*(1), 53–68.

Ganguly, J., Freed, A. M., & Saxena, S. K. (2009). Density profiles of oceanic slabs and surrounding mantle: Integrated thermodynamic and thermal modeling, and implications for the fate of slabs at the 660 km discontinuity. *Physics of the Earth and Planetary Interiors*, *172*(3), 257–267. https://doi.org/10.1016/j.pepi.2008.10.005

Hogrefe, A., Rubie, D. C., Sharp, T. G., & Seifert, F. (1994). Metastability of enstatite in deep subducting lithosphere. *Nature*, *372*(6504), 351–353. https://doi.org/10.1038/372351a0

HughJones, D., Sharp, T., Angel, R., & Woodland, A. (1996). The transition of orthoferrosilite to high-pressure *C2/c* clinoferrosilite at ambient temperature. *European Journal of Mineralogy*, *8*(6), 1337–1345. https://doi.org/10.1127/ejm/8/6/1337

Irifune, T., & Ringwood, A. E. (1987). Phase transformations in a harzburgite composition to 26 GPa: Implications for dynamical behaviour of the subducting slab. *Earth and Planetary Science Letters*, *86*(2), 365–376. https://doi.org/10.1016/0012-821X(87)90233-0

Ishii, T., & Ohtani, E. (2021). Dry metastable olivine and slab deformation in a wet subducting slab. *Nature Geoscience*, *14*(7), 526–530. https://doi.org/10.1038/s41561-021-00756-7

Jackson, J. M., Palko, J. W., Andrault, D., Sinogeikin, S. V., Lakshtanov, D. L., Wang, J. Y., et al. (2003). Thermal expansion of natural orthoenstatite to 1473 K. *European Journal of Mineralogy*, *15*(3), 469–473. https://doi.org/10.1127/0935-1221/2003/0015-0469

Jackson, J. M., Sinogeikin, S. V., & Bass, J. D. (1999). Elasticity of $MgSiO_3$ orthoenstatite, *American Mineralogist*, *84*(4), 677–680. https://doi.org/10.2138/am-1999-0421

Jackson, J. M., Sinogeikin, S. V., & Bass, J. D. (2007). Sound velocities and single-crystal elasticity of orthoenstatite to 1073 K at ambient pressure. *Physics of the Earth and Planetary Interiors*, *161*(1), 1–12. https://doi.org/10.1016/j.pepi.2006.11.002

Jackson, J. M., Sinogeikin, S. V., Carpenter, M. A., & Bass, J. D. (2004). Novel phase transition in orthoenstatite. *American Mineralogist*, *89*(1), 239–244. https://doi.org/10.2138/am-2004-0128

Jiang, G., Zhao, D., & Zhang, G. (2008). Seismic evidence for a metastable olivine wedge in the subducting Pacific slab under Japan Sea. *Earth and Planetary Science Letters*, *270*(3), 300–307. https://doi.org/10.1016/j.epsl.2008.03.037

Kaneshima, S., Okamoto, T., & Takenaka, H. (2007). Evidence for a metastable olivine wedge inside the subducted Mariana slab. *Earth and Planetary Science Letters*, *258*(1), 219–227. https://doi.org/10.1016/j.epsl.2007.03.035

Katsura, T., Yamada, H., Nishikawa, O., Song, M., Kubo, A., Shinmei, T., et al. (2004). Olivine-wadsleyite transition in the system $(Mg, Fe)_2SiO_4$. *Journal of Geophysical Research*, *109*(B2), B02209. https://doi.org/10.1029/2003JB002438

Kawakatsu, H., & Yoshioka, S. (2011). Metastable olivine wedge and deep dry cold slab beneath southwest Japan. *Earth and Planetary Science Letters*, *303*(1), 1–10. https://doi.org/10.1016/j.epsl.2011.01.008

King, S. D., Frost, D. J., & Rubie, D. C. (2015). Why cold slabs stagnate in the transition zone. *Geology*, *43*(3), 231–234. https://doi.org/10.1130/g36320.1

Kirby, S. H., Stein, S., Okal, E. A., & Rubie, D. C. (1996). Metastable mantle phase transformations and deep earthquakes in subducting oceanic lithosphere. *Reviews of Geophysics*, *34*(2), 261–306. https://doi.org/10.1029/96RG01050

Kumazawa, M. (1969). The elastic constants of single-crystal orthopyroxene. *Journal of Geophysical Research*, *74*(25), 5973–5980. https://doi.org/10.1029/JB074i025p05973

Kung, J., Li, B. S., Uchida, T., Wang, Y. B., Neuville, D., & Liebermann, R. C. (2004). In situ measurements of sound velocities and densities across the orthopyroxene -> high-pressure clinopyroxene transition in $MgSiO_3$ at high pressure. *Physics of the Earth and Planetary Interiors*, *147*(1), 27–44. https://doi.org/10.1016/j.pepi.2004.05.008

Li, B., & Neuville, D. R. (2010). Elasticity of diopside to 8 GPa and 1073 K and implications for the upper mantle. *Physics of the Earth and Planetary Interiors*, *183*(3), 398–403. https://doi.org/10.1016/j.pepi.2010.08.009

Lidaka, T., & Suetsugu, D. (1992). Seismological evidence for metastable olivine inside a subducting slab. *Nature*, *356*(6370), 593–595. https://doi.org/10.1038/356593a0

Lin, C.-C. (2004). Pressure-induced polymorphism in enstatite ($MgSiO_3$) at room temperature: Clinoenstatite and orthoenstatite. *Journal of Physics and Chemistry of Solids*, *65*(5), 913–921. https://doi.org/10.1016/j.jpcs.2003.09.028

Liu, K. H., Gao, S. S., Gao, Y., & Wu, J. (2008). Shear wave splitting and mantle flow associated with the deflected Pacific slab beneath northeast Asia. *Journal of Geophysical Research*, *113*(B1), B01305. https://doi.org/10.1029/2007JB005178

Liu, W., & Li, B. (2006). Thermal equation of state of $(Mg_{0.9}Fe_{0.1})_2SiO_4$ olivine. *Physics of the Earth and Planetary Interiors*, *157*(3), 188–195. https://doi.org/10.1016/j.pepi.2006.04.003

Mao, Z., Fan, D., Lin, J.-F., Yang, J., Tkachev, S. N., Zhuravlev, K., & Prakapenka, V. B. (2015). Elasticity of single-crystal olivine at high pressures and temperatures. *Earth and Planetary Science Letters*, *426*, 204–215. https://doi.org/10.1016/j.epsl.2015.06.045

Mosenfelder, J. L., Marton, F. C., Ross, C. R., Kerschhofer, L., & Rubie, D. C. (2001). Experimental constraints on the depth of olivine metastability in subducting lithosphere. *Physics of the Earth and Planetary Interiors*, *127*(1), 165–180. https://doi.org/10.1016/S0031-9201(01)00226-6

Nishi, M., Kubo, T., Ohfuji, H., Kato, T., Nishihara, Y., & Irifune, T. (2013). Slow Si-Al interdiffusion in garnet and stagnation of subducting slabs. *Earth and Planetary Science Letters*, *361*, 44–49. https://doi.org/10.1016/j.epsl.2012.11.022

Pankow, K. L., Williams, Q., & Lay, T. (2002). Using shear wave amplitude patterns to detect metastable olivine in subducted slabs. *Journal of Geophysical Research*, *107*(B6), ESE2-1–ESE2-15. https://doi.org/10.1029/2001JB000608

Raterron, P., Chen, J., & Weidner, D. J. (2002). A process for low-temperature olivine-spinel transition under quasi-hydrostatic stress. *Geophysical Research Letters*, *29*(10), 3631–3634. https://doi.org/10.1029/2002GL015003

Raye, U., Anthony, E. Y., Stern, R. J., Kimura, J.-I., Ren, M., Qing, C., & Tani, K. (2011). Composition of the mantle lithosphere beneath south-central Laurentia: Evidence from peridotite xenoliths, Knippa, Texas. *Geosphere*, *7*(3), 710–723. https://doi.org/10.1130/ges00618.1

Reynard, B., Bass, J. D., & Brenizer, J. (2010). High-temperature elastic softening of orthopyroxene and seismic properties of the lithospheric upper mantle. *Geophysical Journal International*, *181*(1), 557–566. https://doi.org/10.1111/j.1365-246X.2010.04524.x

Ringwood, A. E., & Irifune, T. (1988). Nature of the 650 km seismic discontinuity: Implications for mantle dynamics and differentiation. *Nature*, *331*(6152), 131–136. https://doi.org/10.1038/331131a0

Sang, L., & Bass, J. D. (2014). Single-crystal elasticity of diopside to 14 GPa by Brillouin scattering. *Physics of the Earth and Planetary Interiors*, *228*, 75–79. https://doi.org/10.1016/j.pepi.2013.12.011

Sata, N., Shen, G., Rivers, M. L., & Sutton, S. R. (2002). Pressure-volume equation of state of the high-pressure *B2* phase of NaCl. *Physical Review B*, *65*(10), 104114. https://doi.org/10.1103/PhysRevB.65.104114

Schutt, D. L., & Lesher, C. E. (2006). Effects of melt depletion on the density and seismic velocity of garnet and spinel lherzolite. *Journal of Geophysical Research*, *111*(B5), B05401. https://doi.org/10.1029/2003JB002950

Singh, A. K. (1993). The lattice strains in a specimen (cubic system) compressed nonhydrostatically in an opposed anvil device. *Journal of Applied Physics*, *73*(9), 4278–4286. https://doi.org/10.1063/1.352809

Sinogeikin, S. V., & Bass, J. D. (1999). Single-crystal elastic properties of chondrodite: Implications for water in the upper mantle. *Physics and Chemistry of Minerals*, *26*(4), 297–303. https://doi.org/10.1007/s002690050189

Speziale, S., & Duffy, T. S. (2002). Single-crystal elastic constants of fluorite (CaF_2) to 9.3 GPa. *Physics and Chemistry of Minerals*, *29*(7), 465–472. https://doi.org/10.1007/s00269-002-0250-x

Tamura, A., & Arai, S. (2006). Harzburgite–dunite–orthopyroxenite suite as a record of supra-subduction zone setting for the Oman ophiolite mantle. *Lithos*, *90*(1), 43–56. https://doi.org/10.1016/j.lithos.2005.12.012

Tono, Y., Fukao, Y., Kunugi, T., & Tsuboi, S. (2009). Seismic anisotropy of the Pacific slab and mantle wedge beneath the Japanese islands. *Journal of Geophysical Research*, *114*(B7), B07307. https://doi.org/10.1029/2009JB006290

Van Mierlo, W. L., Langenhorst, F., Frost, D. J., & Rubie, D. C. (2013). Stagnation of subducting slabs in the transition zone due to slow diffusion in majoritic garnet. *Nature Geoscience*, *6*(5), 400–403. https://doi.org/10.1038/ngeo1772

Webb, S. L., & Jackson, I. (1993). The pressure-dependence of the elastic-modili of single-crystal orthopyroxene ($Mg_{0.8}Fe_{0.2}$)SiO_3. *European Journal of Mineralogy*, *5*(6), 1111–1119. https://doi.org/10.1127/ejm/5/6/1111

Weidner, D. J., & Vaughan, M. T. (1982). Elasticity of pyroxenes: Effects of composition versus crystal structure. *Journal of Geophysical Research*, *87*(B11), 9349–9353. https://doi.org/10.1029/JB087iB11p09349

Weidner, D. J., Wang, H., & Ito, J. (1978). Elasticity of orthoenstatite. *Physics of the Earth and Planetary Interiors*, *17*(2), P7–P13. https://doi.org/10.1016/0031-9201(78)90043-2

Xu, J., Fan, D., Zhang, D., Guo, X., Zhou, W., & Dera, P. K. (2020). Phase transition of enstatite-ferrosilite solid solutions at high pressure and high temperature: Constraints on metastable orthopyroxene in cold subduction. *Geophysical Research Letters*, *47*(12), e2020GL087363. https://doi.org/10.1029/2020gl087363

Xu, J., Fan, D., Zhang, D., Ma, M., Zhou, Y., Tkachev, S. N., et al. (2022). Phase transitions of Fe-Al- and Ca-bearing orthopyroxenes at high pressure and high temperature: Implications for metastable orthopyroxenes in stagnant slabs. *Journal of Geophysical Research: Solid Earth*, *127*(1), e2021JB023133. https://doi.org/10.1029/2021JB023133

Xu, J., Zhang, D., Fan, D., Zhang, J. S., Hu, Y., Guo, X., et al. (2018). Phase transitions in orthoenstatite and subduction zone dynamics: Effects of water and transition metal ions. *Journal of Geophysical Research: Solid Earth*, *123*(4), 2723–2737. https://doi.org/10.1002/2017jb015169

Zhang, D., Jackson, J. M., Chen, B., Sturhahn, W., Zhao, J., Yan, J., & Caracas, R. (2013). Elasticity and lattice dynamics of enstatite at high pressure. *Journal of Geophysical Research: Solid Earth*, *118*(8), 4071–4082. https://doi.org/10.1002/jgrb.50303

Zhang, J., Li, B., Utsumi, W., & Liebermann, R. C. (1996). In situ X-ray observations of the coesite-stishovite transition: Reversed phase boundary and kinetics. *Physics and Chemistry of Minerals*, *23*(1), 1–10. https://doi.org/10.1007/BF00202987

Zhang, J. S., & Bass, J. D. (2016). Single-crystal elasticity of natural Fe-bearing orthoenstatite across a high-pressure phase transition. *Geophysical Research Letters*, *43*(16), 8473–8481. https://doi.org/10.1002/2016gl069963

Zhang, J. S., Dera, P., & Bass, J. D. (2012). A new high-pressure phase transition in natural Fe-bearing orthoenstatite. *American Mineralogist*, *97*(7), 1070–1074. https://doi.org/10.2138/am.2012.4072

Zhang, J. S., Reynard, B., Montagnac, G., & Bass, J. D. (2014). Pressure-induced *Pbca–P2*$_1$*/c* phase transition of natural orthoenstatite: The effect of high temperature and its geophysical implications. *Physics of the Earth and Planetary Interiors*, *228*, 150–159. https://doi.org/10.1016/j.pepi.2013.09.008

Zhao, Y., Schiferl, D., & Shankland, T. J. (1995). A high P-T single-crystal X-ray diffraction study of thermoelasticity of $MgSiO_3$ orthoenstatite. *Physics and Chemistry of Minerals*, *22*(6), 393–398. https://doi.org/10.1007/BF00213337

References From the Supporting Information

Akaogi, M., Ito, E., & Navrotsky, A. (1989). Olivine-modified spinel-spinel transitions in the system Mg_2SiO_4-Fe_2SiO_4: Calorimetric measurements, thermochemical calculation, and geophysical application. *Journal of Geophysical Research*, *94*(B11), 15671–15685. https://doi.org/10.1029/JB094iB11p15671

Greaux, S., Irifune, T., Higo, Y., Tange, Y., Arimoto, T., Liu, Z. D., & Yamada, A. (2019). Sound velocity of $CaSiO_3$ perovskite suggests the presence of basaltic crust in the Earth's lower mantle. *Nature*, *565*(7738), 218–221. https://doi.org/10.1038/s41586-018-0816-5

Irifune, T. (1987). An experimental investigation of the pyroxene-garnet transformation in a pyrolite composition and its bearing on the constitution of the mantle. *Physics of the Earth and Planetary Interiors*, *45*(4), 324–336. https://doi.org/10.1016/0031-9201(87)90040-9

Irifune, T., Sekine, T., Ringwood, A. E., & Hibberson, W. O. (1986). The eclogite-garnetite transformation at high pressure and some geophysical implications. *Earth and Planetary Science Letters*, *77*(2), 245–256. https://doi.org/10.1016/0012-821X(86)90165-2

Kung, J., Li, B., Uchida, T., & Wang, Y. (2005). In-situ elasticity measurement for the unquenchable high-pressure clinopyroxene phase: Implication for the upper mantle. *Geophysical Research Letters*, *32*(1), L01307. https://doi.org/10.1029/2004GL021661

Lu, C., Mao, Z., Lin, J.-F., Zhuravlev, K. K., Tkachev, S. N., & Prakapenka, V. B. (2013). Elasticity of single-crystal iron-bearing pyrope up to 20 GPa and 750 K. *Earth and Planetary Science Letters*, *361*, 134–142. https://doi.org/10.1016/j.epsl.2012.11.041

Mao, Z., Jacobsen, S. D., Jiang, F., Smyth, J. R., Holl, C. M., & Duffy, T. S. (2008). Elasticity of hydrous wadsleyite to 12 GPa: Implications for Earth's transition zone. *Geophysical Research Letters*, *35*(21), L21305. https://doi.org/10.1029/2008GL035618

Mao, Z., Jacobsen, S. D., Jiang, F., Smyth, J. R., Holl, C. M., Frost, D. J., & Duffy, T. S. (2008). Single-crystal elasticity of wadsleyites, β-Mg_2SiO_4, containing 0.37–1.66 wt.% H_2O. *Earth and Planetary Science Letters*, *266*(1), 78–89. https://doi.org/10.1016/j.epsl.2007.10.045

Ricolleau, A., Perrillat, J.-P., Fiquet, G., Daniel, I., Matas, J., Addad, A., et al. (2010). Phase relations and equation of state of a natural MORB: Implications for the density profile of subducted oceanic crust in the Earth's lower mantle. *Journal of Geophysical Research*, *115*(B8), B08202. https://doi.org/10.1029/2009JB006709

Saikia, A., Frost, D. J., & Rubie, D. C. (2008). Splitting of the 520-kilometer seismic discontinuity and chemical heterogeneity in the mantle. *Science*, *319*(5869), 1515–1518. https://doi.org/10.1126/science.1152818

Sinogeikin, S. V., & Bass, J. D. (2000). Single-crystal elasticity of pyrope and MgO to 20 GPa by Brillouin scattering in the diamond cell. *Physics of the Earth and Planetary Interiors*, *120*(1), 43–62. https://doi.org/10.1016/S0031-9201(00)00143-6

Sinogeikin, S. V., Bass, J. D., & Katsura, T. (2003). Single-crystal elasticity of ringwoodite to high pressures and high temperatures: Implications for 520 km seismic discontinuity. *Physics of the Earth and Planetary Interiors*, *136*(1), 41–66. https://doi.org/10.1016/S0031-9201(03)00022-0

Wang, J., Bass, J. D., & Kastura, T. (2014). Elastic properties of iron-bearing wadsleyite to 17.7 GPa: Implications for mantle mineral models. *Physics of the Earth and Planetary Interiors*, *228*, 92–96. https://doi.org/10.1016/j.pepi.2014.01.015